sustainability

MDPI

Article

Electric Resistance Sintering of Al-TiO_2-Gr Hybrid Composites and Its Characterization

Salman Ansari [1], Sajjad Arif [1,*], Akhter H. Ansari [1], Abdul Samad [1], Haitham Hadidi [2] and Muhammed Muaz [1]

[1] Department of Mechanical Engineering, Aligarh Muslim University, Aligarh 202002, India
[2] Department of Mechanical Engineering, Jazan University, Jazan P.O. Box 114, Saudi Arabia
* Correspondence: sajjad.aarif@gmail.com; Tel.: +91-9760228851

Abstract: In the present work, Al-TiO_2-Gr hybrid composites were fabricated through a sustainable manufacturing approach, i.e., ERS (Electric Resistance Sintering) technique. In this experimental work, sintering is performed in a high-density graphite die, which also works as a heating element. The green compacts kept in the graphite die are sintered in two ways simultaneously (conduction and resistance heating). This facilitated the accomplishment of the sintering at a lower current (300–500 A). The aluminum (Al) was reinforced with 9 wt. % TiO_2 (rutile) nanoparticles and 3 wt. % graphite microparticles to synthesize a self-lubricated high wear resistance material. Mechanical properties such as density, hardness, and wear loss of the Al-TiO_2-Gr hybrid composite were investigated. Scanning electron microscopy (SEM), Energy-dispersive X-ray spectroscopy (EDS), and X-ray diffraction (XRD) were performed for microstructural investigation. The experiments were performed according to the Taguchi design of the experiment, where three input process parameters (temperature, holding time, and sintering load) were taken to fabricate the Al-TiO_2-Gr composite. The sintering temperature of 550 °C resulted in the maximum value of mean sintered density (approx. 2.45 gm/cm^3). The holding time of 10 min for the sintering resulted in the maximum value of mean sintered density and mean hardness (HRB 53.5). The mean value of wear loss was found to be minimum for the composites sintered at 600 °C for 10 min. The maximum value of the sintering load (800 N) revealed better density and hardness. Worn surfaces and wear debris were also analyzed with the help of SEM images. The sintering temperature of 600 °C resulted in imparting more wear resistance which was proved by smooth surfaces, micro-cutting, and fewer crates, grooves, and smaller pits.

Keywords: sustainable manufacturing; electric resistance sintering; aluminium metal matrix composite; characterization

check for updates

Citation: Ansari, S.; Arif, S.; Ansari, A.H.; Samad, A.; Hadidi, H.; Muaz, M. Electric Resistance Sintering of Al-TiO_2-Gr Hybrid Composites and Its Characterization. *Sustainability* **2022**, *14*, 12980. https://doi.org/10.3390/su142012980

Academic Editor: Joshua M. Pearce

Received: 25 August 2022
Accepted: 6 October 2022
Published: 11 October 2022

Publisher's Note: MDPI stays neutral with regard to jurisdictional claims in published maps and institutional affiliations.

Copyright: © 2022 by the authors. Licensee MDPI, Basel, Switzerland. This article is an open access article distributed under the terms and conditions of the Creative Commons Attribution (CC BY) license (https://creativecommons.org/licenses/by/4.0/).

1. Introduction

Aluminium metal matrix composites (AMCs) have always been in high demand in the automotive, aerospace, and mineral processing industries due to their superior strength-to-weight ratio [1], high strength and modulus, good ductility, excellent wear, corrosion resistance [2], high temperature creep resistance, low coefficient of thermal expansion, and better fatigue strength, etc. [3]. The mechanical properties of composites are mainly dependent upon the type of reinforcement, particle size and fraction and processing method [4,5]. Various manufacturing techniques, such as stir casting, mechanical alloying, and powder metallurgy, are adopted to fabricate AMCs [6]. Each manufacturing approach has a unique set of benefits and drawbacks [7]. For instance, the casting process offers a clear advantage in terms of low-cost manufacturing, but non-uniform dispersion of reinforcement and undesired interfacial reactions result in a loss of mechanical properties [2,7]. On the other hand, powder metallurgy (PM) has gained popularity in the production of AMCs because of its potential advantages, such as uniform dispersion of reinforcements in matrix material, and low possibility of developing any intermetallic phase due to processing at a lower temperature than casting. Further, the fabrication of near-net-shaped products and the

ability to produce parts of complex shapes to close tolerance are the unique feature of the powder metallurgy process [8–10]. The final properties of the product are significantly influenced by the sintering procedure as well as its processing variables like temperature, holding time, pressure, etc. [7,11]. Therefore, powder metallurgists, in collaboration with material scientists, are continuously putting effort into developing efficient and improved sintering techniques to achieve superior microstructures and mechanical characteristics [7]. In the conventional sintering method, slow heating rates and prolonged holding times typically cause excessive grain coarsening. In addition, the non-uniform distribution of heat creates a thermal gradient in the specimen that results in internal stresses in the product [9,11]. In recent years, some advanced sintering techniques such as microwave (MW), laser, electric resistance, and spark plasma sintering (SPS) have been utilized to sinter AMCs [11,12]. These non-conventional sintering techniques offer many advantages over conventional heating methods, including improved diffusion processes, high heating rates, shorter processing times, and better control over microstructure during processing, with improved properties in the final products [11,12]. The SPS technique is widely used for the fabrication of MMCs [11,13]. However, the SPS equipment is too expensive to meet the demands of mass production in the industrial sector. Furthermore, with long-term continuous operation, pulsed electric current generators are easily destroyed. Therefore, it is required to develop a super-fast consolidation, simple and low-cost sintering technique [13]. Previous works by researchers on non-conventional sintering showed that ERS is a faster sintering technique than microwave and SPS [9,14,15]. S Maki et al. [16] fabricated Cu–Al_2O_3 composites by the ERS technique applying power input up to 12 kW and Voltage of 8–10 V. A. H. Ansari et al. [17] sintered brass by applying DC of 0.4–1.0 kA on voltage 12 V. M. A. Lagos et al. [15] developed an ERS process for the sintering of hard metals. They fabricated WC-Co composite applying current 35 kA on 40 V. F. G. Cuevas et al. [18] investigated the effect of different ceramic dies in ERS. M. B. N. Shaikh, et al. [9] sintered Al-SiC composite by applying the DC of 0.8–1 kA at a low voltage of range 3–5 V using a steel die lined with an alumina tube to insulate the green compact.

Thus, previous works show that a DC of very high intensity, in the range of 1–10 kA, having a low voltage of the range of 3–12 V is required for ERS. A ceramic die is generally used in ERS [18], in which powder or green compact is placed for sintering by applying DC [9]. The resistance of green compact causes to generate heat according to Joule's heating [9,15]. Sometimes, the porosity of the loose powder kept in the ceramic die causes a problem, and the current of lower intensity on low voltage does not flow. In the current work, a high-density graphite die is used in place of a ceramic die, and it gives a favorable result. In tribological applications, hybrid AMCs reinforced with micro, and nano-sized particles are being explored due to their advantages, such as micro-sized reinforcements supporting the skeleton of soft Al matrix and nano-sized reinforcements improving mechanical characteristics by promoting fine grain structure and preventing dislocation movements [6]. In comparison to micron-sized reinforcements, the inclusion of a small proportion of nanoparticles can increase the characteristics of Al without affecting its ductility [7]. Automobile components made of AMCs utilizing SiC, Al_2O_3, B_4N, TiC, etc., are preferred in vehicles so that weight can be reduced and fuel efficiency can be increased, along with providing good wear resistance and high cycle fatigue resistance at moderately elevated temperatures [19]. Researchers have paid little attention to the use of TiO_2 as reinforcement in AMCs, despite its high hardness, and modulus, as well as excellent wear and corrosion resistance [20,21]. Rutile is a natural form of TiO_2 mineral that is economical and readily available [22]. The incorporation of any solid lubricant is advantageous under dry sliding conditions because it forms a thin layer of lubricant that reduces wear loss [6]. For further enhancement of tribological performance, graphite is the most suitable and frequently used material because its inclusion in AMCs also causes improved wear resistance and machinability, excellent anti-seizure effects, low thermal expansion, and high damping capacity in the product [6,23]. Therefore, in this work, the Al matrix is reinforced with 9 wt. % TiO_2 (rutile) nanoparticles and 3 wt. % graphite micro

particles to fabricate a self-lubricating Al-TiO_2-Gr hybrid composite which would be useful for bearings and bushing production.

According to the best of the authors' knowledge, there has been no research on ERS using the high-density graphite die in powder metallurgy. In addition, there has been no work on the fabrication of an Al-TiO_2-Gr composite having the above-mentioned composition prepared by this new approach in ERS. L25 array Taguchi models were used for the optimization of the process parameters of ERS. Further, the mechanical properties such as density, hardness, and wear loss are also investigated as well as the effect of sintering temperature, holding time, and sintering pressure on these properties are also analyzed. Worn surfaces and wear debris are analyzed through SEM images to understand the mechanism of wear.

2. Materials and Methods

2.1. Raw Materials and Their Characteristics

The pure Al and graphite powder was purchased from Central Drug House Pvt. Ltd., India. Nano-sized particles of TiO_2 (rutile) were obtained from Sisco Research Laboratories India. Some usual properties of these powders are shown in Table 1.

Table 1. Specifications of as-received powders.

Powder	Powder Type	Mean Size (μm)	Density (g/cm^3)	Melting Point (°C)
Al	Elemental	74	2.7	660
Gr	Elemental	100	1.9	3652–3697
TiO_2	Ceramic	Nano-sized	4.23	1843

These powders were used with the following composition: 88 wt. % Al, 9 wt. % TiO_2 and 3 wt. % Gr. To achieve the above composition, the weighing of powders was done carefully on a digital balance (Precisa, Model No ES225SM-DRSCS, Dietikon, Switzerland) with readability up to 5 decimal places in grams. Weighted powders were sealed air-tight in a stainless-steel container and mixed properly at an ambient temperature of 25 °C in a low-energy vibratory ball mill (Fritsch, Pulverisette MM-1552, Germany) for 30 min at a constant rotational speed of 300 rpm. High stainless steel (HSS) balls of 10 mm diameter were used as grinding media in this blending process. Ball-to-powder ratio (BPR) was kept at 10:1 to reduce the chance of clustering in these powders. To avoid the excessive cold welding of the aluminium particles among themselves as well as onto the surface of balls and vials, 0.5 wt. % of stearic acid ($C_{18}H_{36}O_2$) was also added to the mixture, which works as a process control agent (PCA) during this mechanical mixing process. The morphological characteristics and elemental composition of powders were investigated using scanning electron microscopy (SEM) equipped with energy-dispersive X-ray spectrometry (EDS) (Jeol, JSM 6510LV-Japan). Different phases present in Al-TiO2-Gr composite powder were identified using an x-ray diffractometer (XRD, Bruker, D8 ADVANCE, USA).

2.2. Preparation of Al-TiO_2-Gr Composites

Mechanically mixed composite powders were compacted through a single-acting uni-axial hydraulic press (Type KE, Sr No. 1327, Kimaya Engineers, India) within a high carbon steel pallet die having a 12 mm internal diameter at an applied pressure of 300 MPa and room temperature of 25 °C. Generally, the cold welding of some Al metal particles along the die wall takes place due to friction during compaction; therefore, to avoid this problem as well as for easy removal of the sample from the die, the curved surfaces of the die cavity and punches were lubricated properly with zinc stearate ($C_{36}H_{70}O_4Zn$) after every compaction. For each run, the sample was kept in the die under pressure for 25 s approximately to minimize the effects of back-pressure produced during compaction.

After cold compaction, green compacts were pre-sintered before ERS. The pre-sintering operation was carried out in a tubular furnace (Ants Innovations Pvt. Ltd. India) at 200 °C for 30 min with a heating rate of 10 °C/minute under the controlled atmosphere of N_2

gas. The pre-sintering facilitates in burning off moisture, additives, etc. and the integrity of the compacts for the sintering is also improved [9]. The heating curve adopted in the pre-sintering is shown in Figure 1. Green compacts were allowed to cool naturally in the tubular furnace.

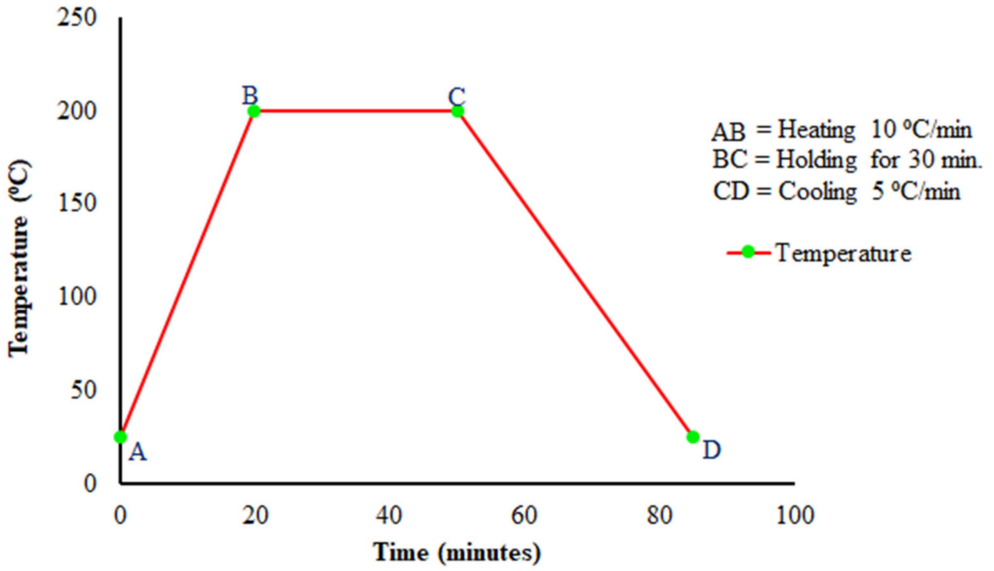

Figure 1. Heating curve during pre-sintering.

For the ERS operation, the pre-sintered compact was placed in high-density graphite die between the upper and lower graphite plunger attached to the copper electrode. The schematic diagram of the ERS setup is shown in Figure 2.

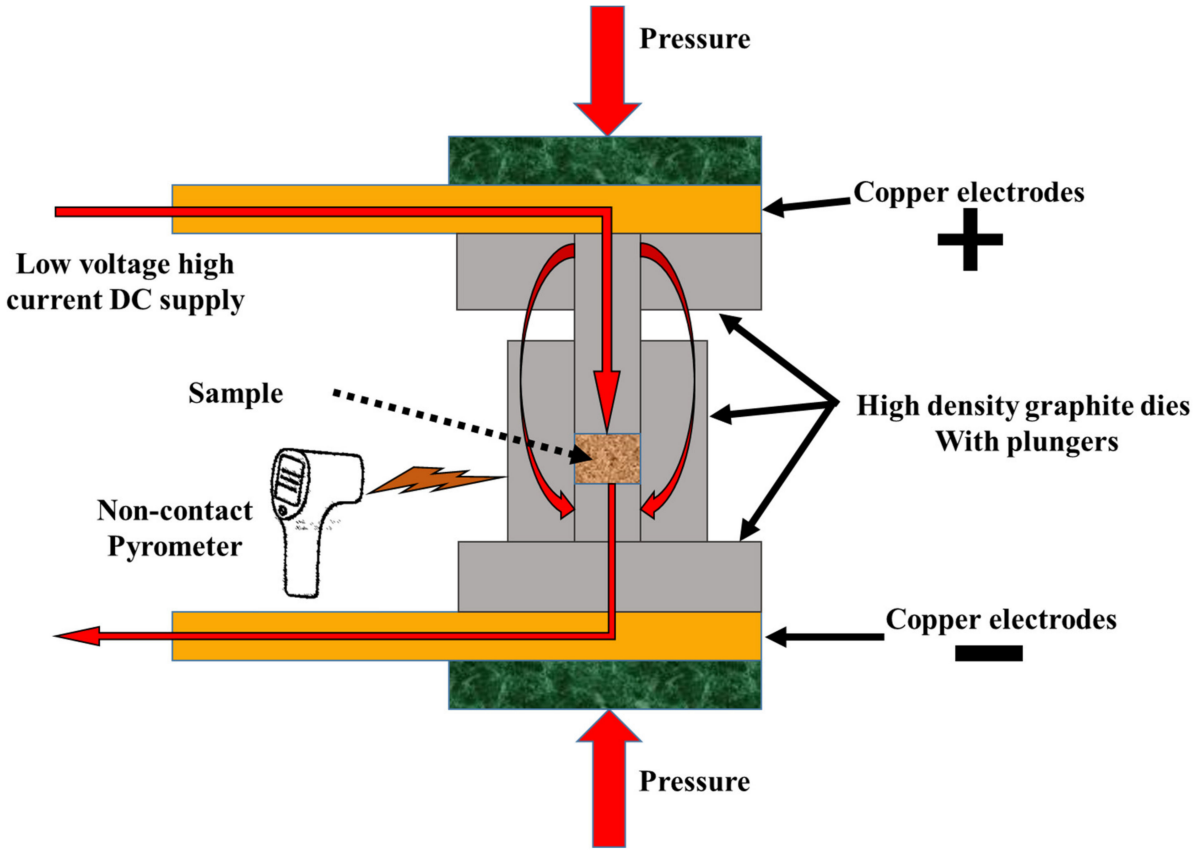

Figure 2. Schematic diagram of ERS setup.

Available AC (220–230 V) is converted into low voltage and high current with the help of a continuously variable autotransformer (Make—Automatic Electric Limited, Mumbai, India) by simple transforming action further, the output is supplied to the rectifier to convert alternating current (AC) into plain direct current (DC). Hence, a plain DC in the range of 200–400 A of low voltage (3–5 V) was obtained that was applied for the sintering of the green compact. The resistance of green compact is caused to generate heat according to Joule's heating [16].

At the same time, the resistance of graphite die, and punches also produced heat when the current passed through it, and hence the graphite die also worked as a heating element. Thus, the sample was heated due to the conduction of heat from the graphite die to the AMC sample, along with resistance heating of the AMC. Hence the sintering happened in both ways simultaneously at a lower intensity of the current (300–500 A). The sintering cabin is shown in Figure 3.

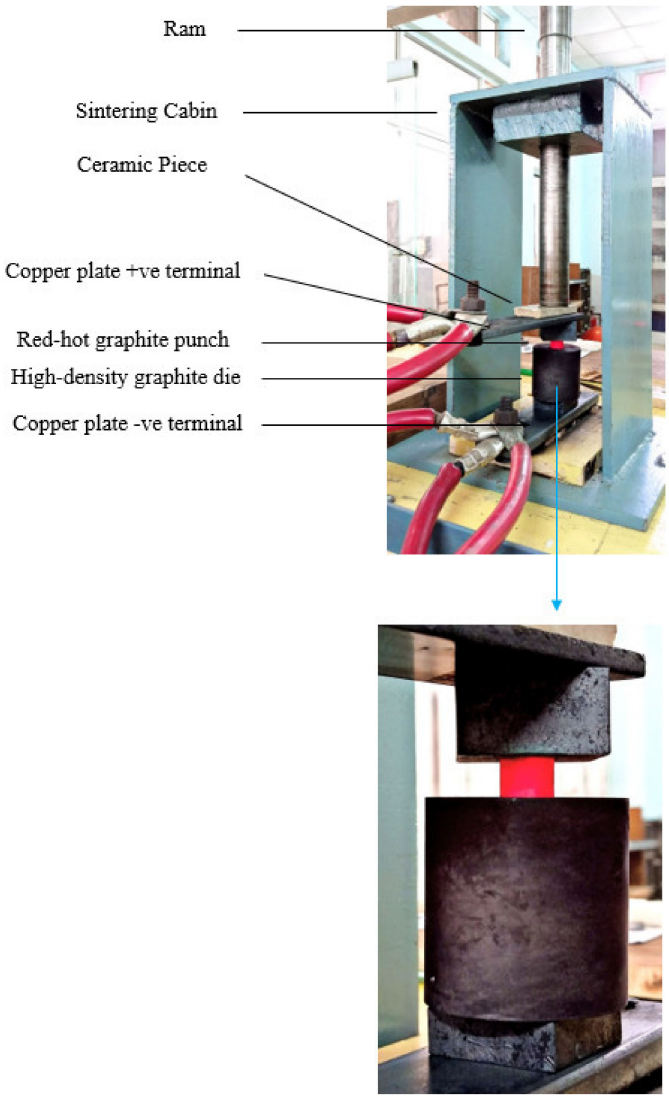

Figure 3. Sintering chamber during the flow of current in a graphite die.

The experiments were performed according to the L25 array of the Taguchi Model. Following these three factors were selected as input process parameters: (i) sintering temperature, (ii) holding time during sintering, and (iii) sintering pressure. Each of these factors had five levels for the analysis of their effect on the properties of the composites. The design of the experiment based on the Taguchi model is shown in Table 2.

Table 2. Design of experiments based on the L25 array of the Taguchi Model.

Sr No.	Sintering Temperature (°C)	Holding Time (min)	Sintering Pressure (MPa)
1.	450	1	0
2.	450	3	1.75
3.	450	5	3.50
4.	450	10	5.25
5.	450	15	7.00
6.	500	1	1.75
7.	500	3	3.50
8.	500	5	5.25
9.	500	10	7.00
10.	500	15	0
11.	550	1	3.50
12.	550	3	5.25
13.	550	5	7.00
14.	550	10	0
15.	550	15	1.75
16.	600	1	5.25
17.	600	3	7.00
18.	600	5	0
19.	600	10	1.75
20.	600	15	3.50
21.	650	1	7.00
22.	650	3	0
23.	650	5	1.75
24.	650	10	3.50
25.	650	15	5.25

2.3. Microstructural Characterization (SEM, XRD, EDS & Optical Micrographs)

SEM images were captured at 15 kV in secondary electron mode at various magnifications. To verify the presence of reinforcing particles (TiO_2 and graphite) in AMCs, a structural phase study of the fabricated composites was performed using an X-ray diffractometer operating at 40 mA current and 20 kV accelerating voltage using CuKα radiation (wavelength λ = 1.5406 Å). To determine the present phase, data were collected at a slow scan speed of 0.02 steps/s with a step size of 0.01° within the scanning angle range $20^\circ \leq 2\theta \leq 80^\circ$. DIFFRAC® plus (Bruker AXS Inc., MA, USA) software was used to process the obtained data. Dispersion of reinforcements in matrix material and homogeneity of AMCs were performed using EDS elemental mapping. Sample preparation is the first step to taking the optical micrographs through a microscope. Sintered compact was mounted with a resin mixed with hardener (Araldite) that facilitates a better and more stable holding during polishing. Initially, the mounted samples were polished with the help of emery papers of grit sizes 180, 220, 320, 400,600, 800, 1000, 1200, and 2000.

Finally, these samples were polished on a single disc polishing machine on synthetic velvet cloth using alumina as grinding media. To reveal the microstructure, polished samples were etched with NaOH solution. The optical micrographs of the polished sample were taken by an inverted metallurgical microscope (Truemet, India).

2.4. Density of the Composites

2.4.1. Theoretical Density

It is the maximum achievable density without any voids. The density of each component and its mass fraction should be known to calculate it. The theoretical density of the composite is calculated analytically according to the following formula [24]

$$\rho_{theo} = \frac{1}{\frac{m_{Al}}{\rho_{Al}} + \frac{m_{TiO_2}}{\rho_{TiO_2}} + \frac{m_{Gr}}{\rho_{Gr}}} \quad (1)$$

where 'm' is the mass fraction of a particular component, and 'ρ' denotes the density.

Applying the above formula, the theoretical density of the composite is calculated as below:

$$\rho_{theo} = \frac{1}{\frac{0.88}{2.7} + \frac{0.09}{4.23} + \frac{0.03}{1.9}}$$

$$\rho_{theo} = 2.7548\ g/cm^3$$

2.4.2. Green Density

The density of the composite just after compaction is termed green density. It is always less than the sintered density and theoretical density.

2.4.3. Sintered Density

Archimedes's principle (ASTM: B962-17) was applied to measure the sintered density of fabricated composites. The density of the composite after the sintering process is termed sintered density. The porosity of the sample gets eliminated during the sintering operation when the mass transportation takes place, and hence the density of the composite gets increased. The efficiency of the sintering process is usually evaluated by sintered density.

2.5. Hardness and Wear Characteristics

Metal hardness is a property that influences how well a metal resists abrasion and wear. The hardness of the fabricated composites was measured by an analog Rockwell hardness tester (Meta Test instrument, New Delhi, India). according to ASTM E18-17 standard. The hardness test was performed as per the condition provided in Table 3.

Table 3. Testing parameter of hardness.

Scale	Load	Indenter	Dwell Time
B	60 kgf.	1/16 inch	20 s

The wear test of the fabricated composites was carried out on a pin-on-disc wear machine (Model: TR-201 CL, Ducom, India) under ASTM G99-95a (reapproved 2000). Dry sliding wear tests, of sample size as per ASTM G99 standard, were conducted. Wear specimen of 12.5 mm dia., and 6 mm thickness was polished with 600 emery paper. A cleaned specimen of fabricated AMC was pressed against a rotating EN32 steel disc (hardness 65HRC) of diameter 80 mm and thickness of 8 mm by applying the 10 N load at the room temperature of about 28 °C on a rotating speed of 450 rpm.

3. Results and Discussions

3.1. Characterizations of the Powders and Composites

The microstructure of the aluminium, TiO_2 (rutile), and graphite powders were investigated using SEM images. SEM micrographs of these powders are presented in Figure 4. Aluminium powders show irregular, cylindrical, droplet, and ligamental morphology, while TiO_2 nanoparticles possess mostly spherical shapes and some irregular shapes with wide size distribution.

The microparticles of graphite have an irregular shape with sharp edges. This variety in the shapes and sizes of these powders will be favorable for the powder consolidation processes [9].

In XRD analysis, peaks of pure Al powder were obtained at diffraction angles 39.1°, 44.50°, 64.9°, and 78.90°. Peak reinforcing particles TiO_2 (rutile) were identified at the diffraction angle of 27.8°, 37.2°, and 55°. And a single peak of graphite was observed at 25.6°.

The XRD graphs of composite powder and fabricated composites are shown in Figure 5. From XRD plots, the presence of Al, TiO_2, and graphite powders is confirmed from their respective peaks in sintered composites.

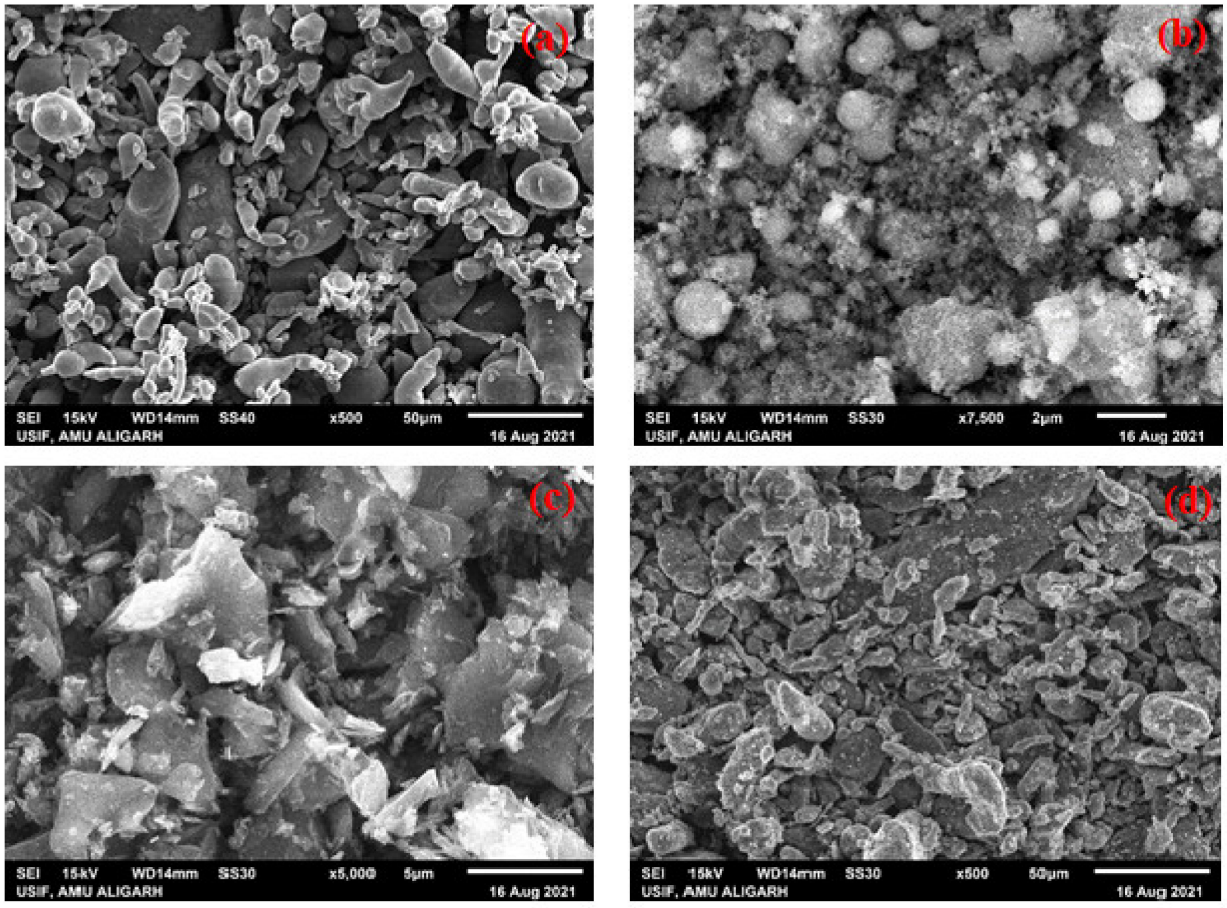

Figure 4. SEM of as-received particles (**a**) Al (**b**) TiO_2—nano and (**c**) Graphite—micro (**d**) Al-TiO_2-Gr powder.

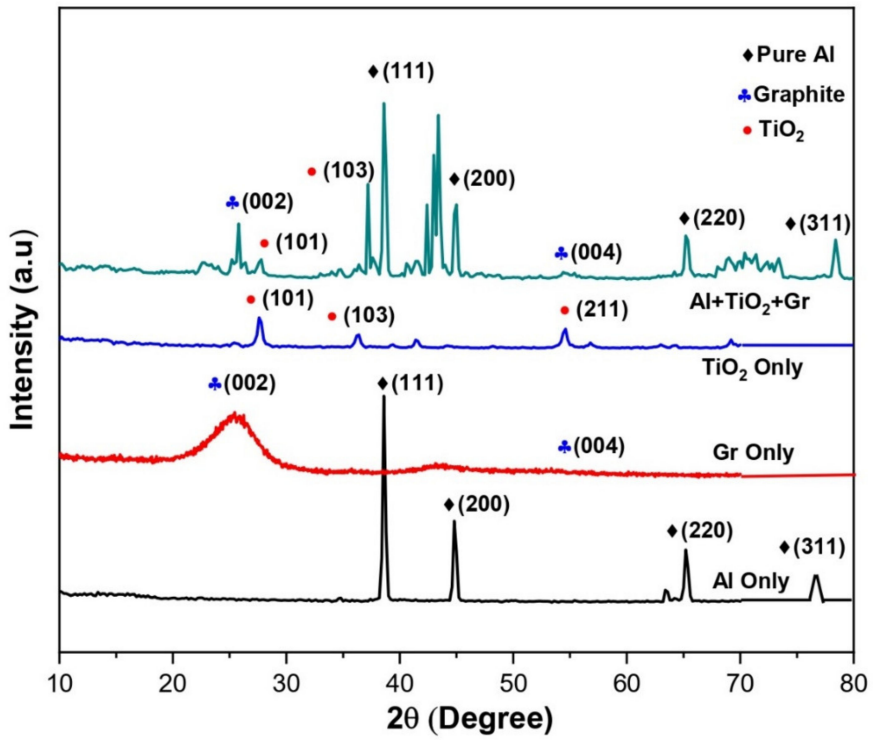

Figure 5. XRD patterns of Al, Gr, TiO_2 and Al + 9% TiO_2 + 3% Gr.

Figure 6 presents the EDS of the Al-TiO_2-Gr composite sintered at 600 °C for 10 min of holding time. The peaks of Al, Ti, C, and O are evident from the EDS report. The wt. % of Al was taken at 88% in the composition, but at a specific location, the EDS result showed 70 wt. % Al in the sample. On the other hand, the result showed 10.02 wt. % C (graphite) while graphite was taken 3 wt. % in the composition of the powder during mixing. The reason behind this variation in wt. % may be the lack of proper mixing of the composite powder. To avoid this deficiency, the milling time should be increased. The atomic percentage of oxygen and Ti elements were 15.54% and 2.93%, respectively. It must be noticed that TiO_2 was the only reinforcement added to AMCs having oxygen. According to the chemical formula of TiO_2, the atomic ratio between Ti and O is 1:2. Hence, for 2.43% of Ti, there should be 4.86% of oxygen. This increased atomic % of oxygen element dictates that oxidation of aluminium has occurred. Figure 7 shows the elemental mapping of the fabricated AMCs. Elemental mapping ensures that there was a lack in the homogeneous mixing of graphite while TiO_2 was distributed uniformly in the matrix material.

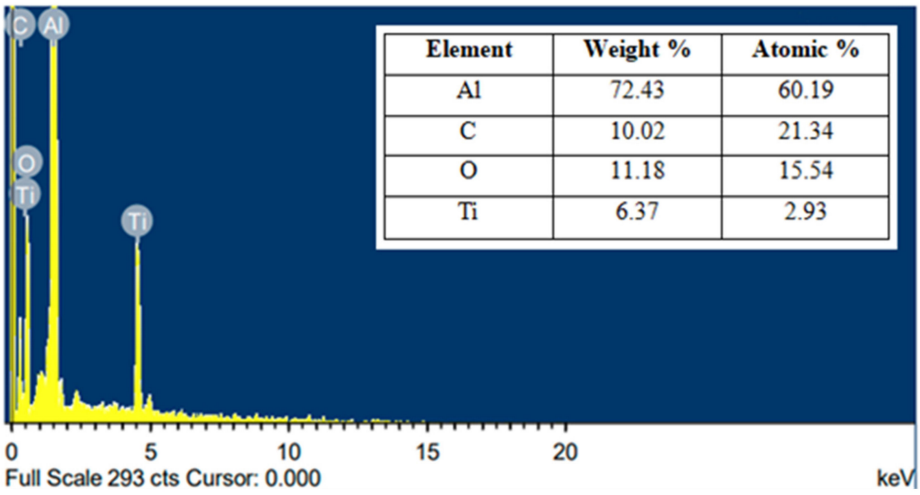

Element	Weight %	Atomic %
Al	72.43	60.19
C	10.02	21.34
O	11.18	15.54
Ti	6.37	2.93

Figure 6. EDS of Al-TiO_2-Gr composite.

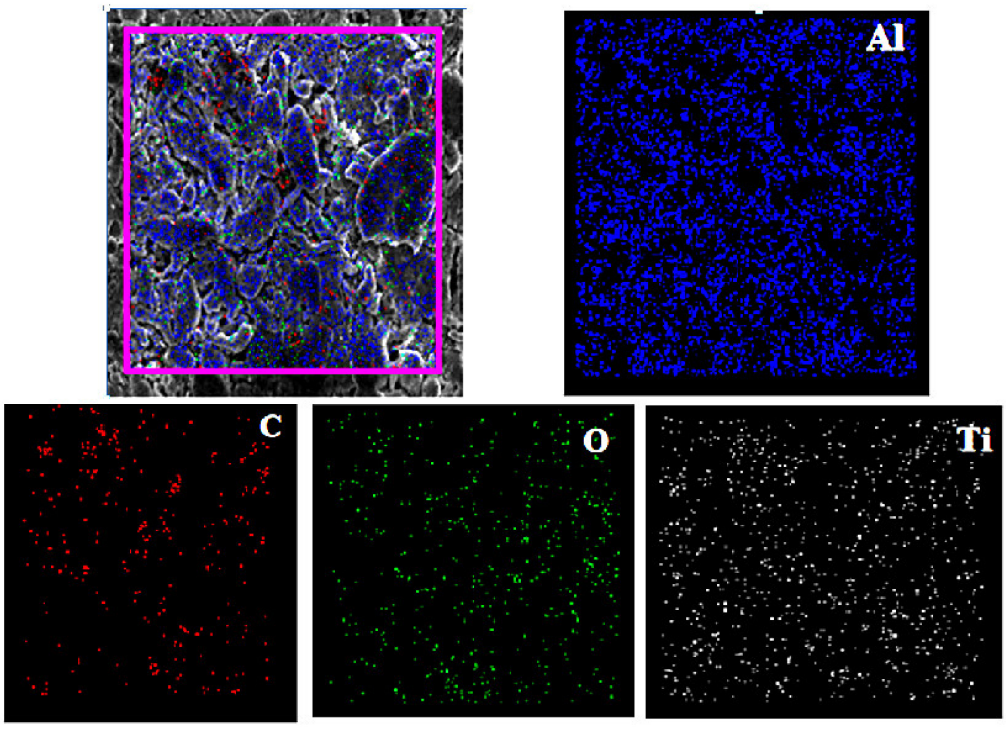

Figure 7. Elemental mapping of Al-TiO_2-Gr composite.

3.2. Optical Micrographs

Two samples sintered at 450 °C and 600 °C through ERS technique were selected for polishing to take optical micrographs. The two micrographs depict that the sample sintered at 450 °C has more porosity than the sample sintered at 600 °C. Thus, higher temperature causes more consolidation of particles. Some large grains were observed in a later one which revealed that grain coarsening has also taken place at the higher sintering temperature. The optical micrographs of these two samples are shown in Figure 8a,b.

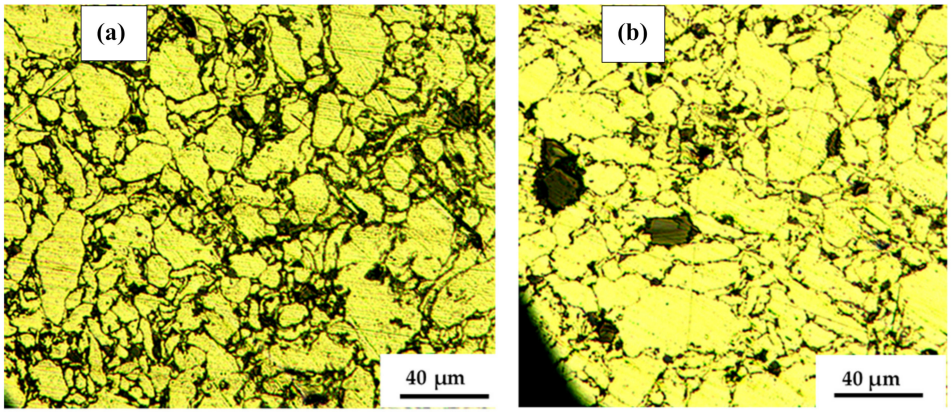

Figure 8. Optical micrographs of composites (**a**) sintered at 450 °C (**b**) sintered at 600 °C.

3.3. Sintered Density

Figure 9 depicts the trend of sintered density for sintering temperature, holding time of sintering, and sintering pressure. It was noticed that for lower sintering temperatures, e.g., 400 °C and 450 °C, the achieved densification in the pellets was very low; even for 400 °C, the improvement in the density was negligible. The reason for this slight change in the sintered density at lower temperatures may be due to lower diffusion rates. Similar findings have been reported by Choudhury et al. [25]. The possible reason for the slight change in the sintered densities could be associated with the fact that the presence of TiO_2 affected the sintering adversely at lower temperatures [26,27]. Further, the densification rate increases for the higher sintering temperature. The maximum sintered density was achieved at 550 °C sintering temperature. This maximum achievement in sintered density is due to fast pores reduction at high temperatures [28]. Lokendar Ram et al. [29] reported that the optimum sintering temperature was 620 °C for Al alloy powder compacted at 350 MPa. Maximum sintered density was obtained in the range of 610–625 °C sintering temperature; they also reported that the rate of densification was highest between 600 °C and 620 °C after 620 °C there was a decrease in the sintered density.

The sintered density was found to be increasing with the holding time of sintering. It may be due to the consolidation of the particles with the initiation of the sintering. It causes an increase in the density of the composites. A longer holding time causes more consolidation. The rate of densification was high in the range of 1 to 5 min of holding time. The rapid change in sintered density in the first 5 min may be attributed to the lower abundance of pores in the composites. Further increase in holding time reduced the rate of densification. It would be due to the following reasons: (a) a larger amount of porosity reduction in the initial stage and, (b) the increase in relative density of the alloy slowed due to grain growth [28].

Figure 9 also depicts the variation in sintered density due to isostatic pressure during processing. The rate of densification is slow in comparison to the densification rate due to the variation in temperature and holding time. From the figure, it is evident that up to 4 MPa applied pressure, sintered density increases sharply. This sharp rise in the density is because of the rearrangement of poorly packed powders and the plastic deformation of soft aluminium particles [30]. Further, high densification may be achieved beyond 4 Mpa may

be due to an increase in compaction pressure leading to an increase in the particle contact area, which alleviates sintering phenomena [31].

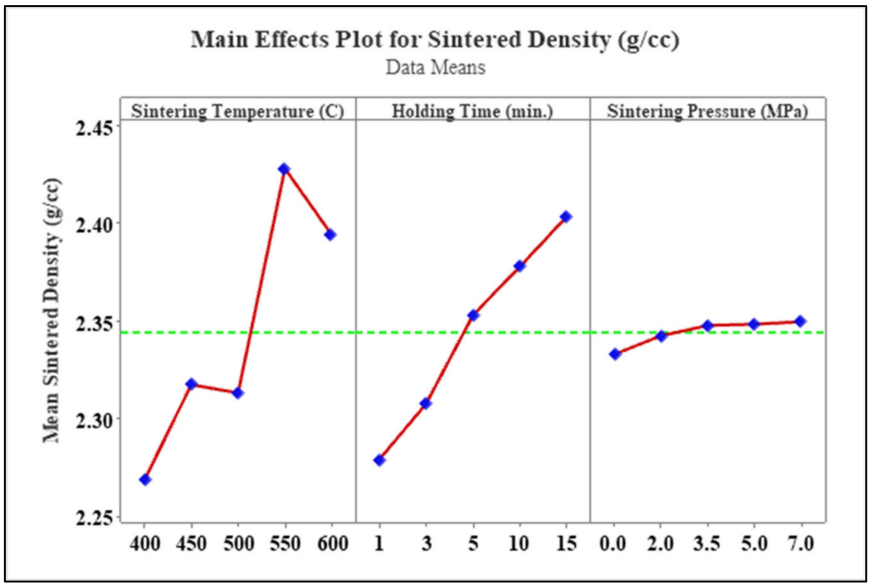

Figure 9. Graph showing the effect of various parameters on sintered density.

3.4. Rockwell Hardness

Figure 10 shows the variation in Rockwell hardness of sintered composite fabricated at various levels of input parameters. The hardness was found to be increasing with the increase in sintering temperature, and the maximum hardness was obtained for the Al-TiO_2-Gr composite sintered at 600 °C. Here it was noticed that the hardness was increasing rapidly between 400 °C and 500 °C; after this range, the slope of hardness was lowered. The rise in the hardness of composites due to the temperature rise may be due to the following reasons: (a) fast reduction of pores at elevated temperature, (b) improvement in the sintered density of the composites [32].

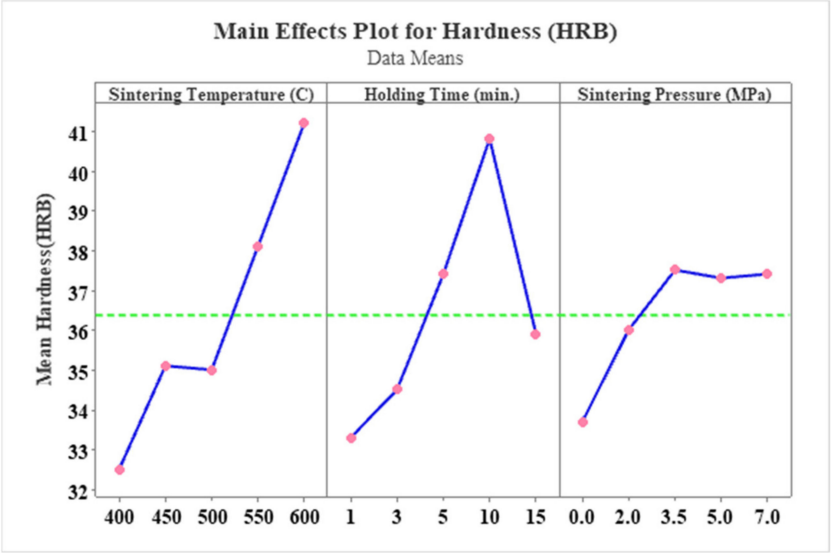

Figure 10. Main effect plot for hardness with temperature, holding time, and sintering pressure.

The trend of variation of hardness for holding time is also positive. This positive gain in the hardness of composites is exhibited due to improved diffusion phenomena at large time intervals [33,34]. Further, the maximum hardness is achieved at a holding time of

10 min, and beyond this, there is a decline in hardness value; it would be due to grain coarsening that started to take place for a longer duration of sintering time [35]. Sintering pressure also caused to increase in the hardness of the AMCs. However, this change in hardness is almost insignificant, as suggested by the mean line depicted in Figure 10. In the present study, the holding time and sintering temperature were observed to be critical parameters to improve the hardness of the composites.

3.5. Wear Loss

The effect of sintering temperature, holding time, and sintering pressure on wear loss was examined and shown in Figure 11. The wear test was performed in dry sliding conditions at the ambient temperature of 27 °C for the sliding parameters of load 10 N, speed 2.0 m/s, and distance 750 m for all samples. Figure 11 reveals the behavior of wear loss of AMCs sintered at various pre-decided process parameters. Wear loss was found to be decreasing with an increase in sintering temperature. AMCs sintered at 600 °C showed minimum wear loss. This maximum resistance in the wear of the composites may be due to the following reasons: (a) proper densification at high temperatures, and (b) maximum gain in hardness at 600 °C [36]. It was noticed that the holding time range from 5 to 15 min was optimum for developing wear resistance in the AMCs. In addition to it, sintering pressure was also a factor that affected the wear loss. As this pressure increased, the wear loss was found to be decreasing. Higher sintering temperature facilitates better inter-particle fusion, which restrains the pull-out of TiO_2 and graphite particles. Therefore, lesser reinforcement particles crammed between surfaces during sliding, reducing third body abrasion wear along nanoparticles of TiO_2 (rutile). Higher temperatures facilitate a strong interfacial bonding with the matrix material and work as a barrier to resist the movement of particles during wear. It also creates a mechanically mixed layer at the surface, working as a load-bearing constituent [9]. Graphite works as a solid lubricant that helps to reduce wear loss during friction [6]. Figure 12 dictates the behavior of wear loss for the hardness of AMCs. The variation in wear loss was found to be according to Archard's law which states that wear resistance is proportional to hardness in other words, wear loss decreases with an increase in hardness [9,37].

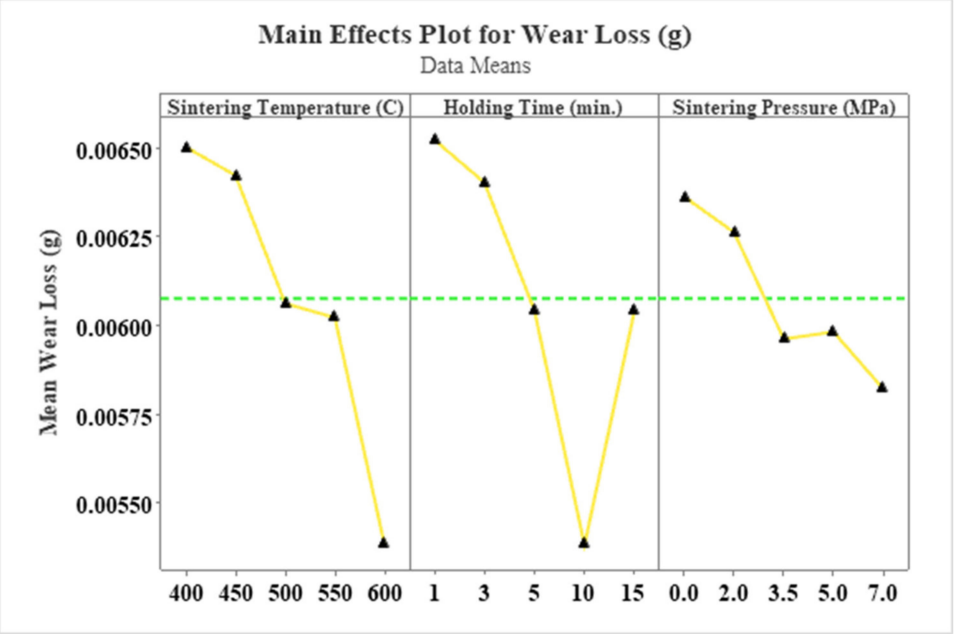

Figure 11. Main effect plot for wear loss with sintering temperature, holding time and sintering pressure.



Figure 12. Wear loss (g) vs Rockwell hardness (HRB).

3.6. Worn Surface Analysis

SEM images were taken of two samples fabricated at different parameters for the analysis of the worn surfaces. Figure 13a shows the worn surface of the Al-TiO_2-Gr composite sintered at 450 °C for 10 min of holding time. Delamination is the most dominant wear mechanism for this sample, as suggested by SEM micrographs. Delamination, adhesive, abrasive, and fretting are some wear mechanisms that are related to the wear behavior of AMCs [38]. Delamination is characterized by excessive material loss from the surface in the form of thin layers. A few significant signs of abrasion are as follows flake-like debris, deep grooves, pits, and craters [37,39]. Figure 13a shows craters, large pits, and fretting wear at various locations. A series of interconnected wear marks and ploughing are also evident on worn-out tracks due to the poor bonding of reinforcing particles in the matrix material. Further, fractured debris in the form of flakes was also seen due to plastic deformation of the contact surface. The heat produced due to sliding also softens the rubbing surface, which further leads to material loss due to the following reasons; (a) severe plastic deformation and (b) reinforcement particles pullout form the embedding locations. [6].

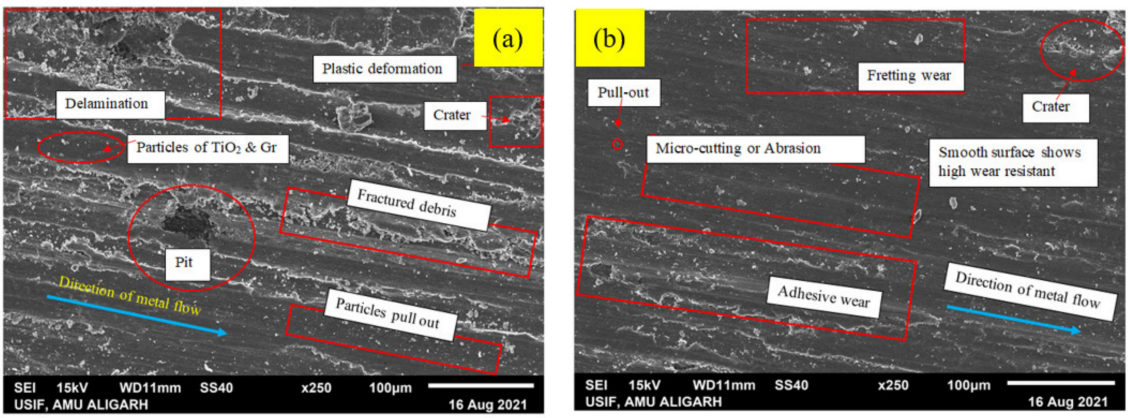

Figure 13. SEM image of Al-TiO_2-Gr composite (**a**) sintered at 450 °C (**b**) sintered at 600 °C.

Figure 13b depicts the worn surface of the same aluminium hybrid composite, which was sintered at 600 °C for 10 min. In this figure, a lesser amount of wear marks, such as ploughing, micro pits, craters, and wider grooves, are seen in comparison to Figure 13a. However, narrow longitudinal grooves and shallower scratches parallel to each are visible, which confirms that abrasion wear has taken place here. Adhesive wear is also identified

by the display of plastic deformation at a few locations. The smooth appearance of the worn surface, along with the restriction of grooves, validate the wear resistance of this composite. The reason behind the high resistance against wear is as follows (a) a higher level of sintering temperature, which resulted in better interfacial bonding between the particles and reinforcement, (b) enough amount of surface energy to accomplish diffusion between the particles and mass transfer [40].

3.7. Wear Debris

As shown in Figure 14a, large flakes like wear debris were formed due to plastic deformation and delamination. Irregular and flaky chips confirm that the adhesive wear mechanism is dominant. Similar findings have been reported in past studies [41,42]. Nano-sized particles of TiO_2 and micro-sized graphite particles were ejected from their place due to poor bonding and were seen in debris, causing a high wear loss. On the other hand, Figure 14b depicts the wear debris of smaller size with some sharp edges in comparison to the previous one. Abrasion wear, in this case, caused a smaller size of debris with fewer amounts of equiaxed flakes. Shaikh et al. [9] reported that densely packed Al-SiC composite sintered through ERS produced small-size wear debris during the wear test in comparison to pure aluminium.

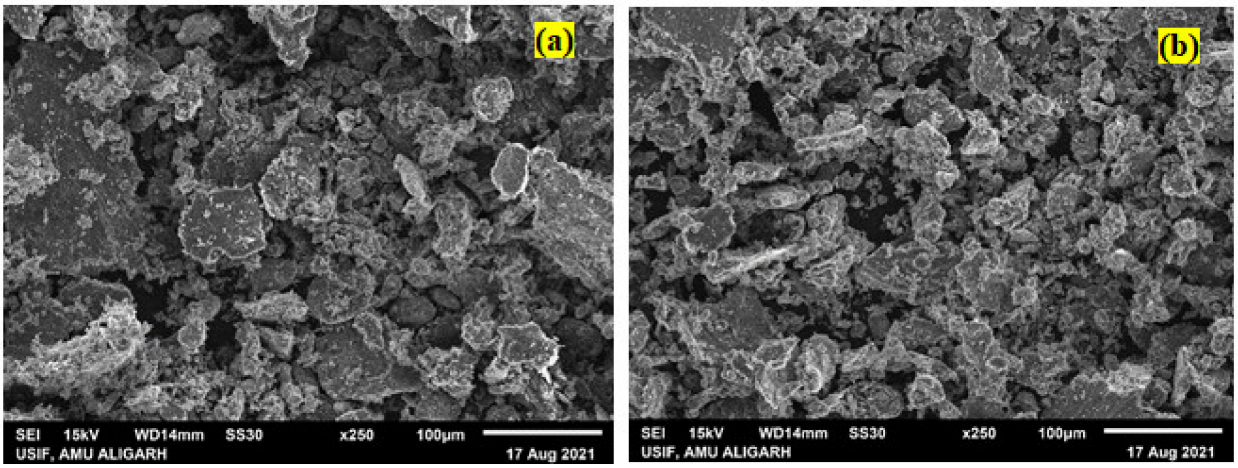

Figure 14. Wear debris of Al-9% TiO_2-3% Gr. (**a**) Sintered at 450 °C for 10 min (**b**) Sintered at 600 °C for 10 min.

4. Conclusions

In this experimental work, AMCs reinforced with 9 wt. % nano sized TiO_2 (rutile) and 3 wt. % micro-sized graphite was produced successfully using ERS method. The main findings of the experimental work are as follows:

- Al-TiO_2-Gr hybrid composites are fabricated using graphite die and applying the current in the ranges of 200–400 A DC and voltage between 3–5 V.
- The XRD, EDS and elemental mapping confirm the validation of synthesized composites. The elemental mapping of the synthesized composite revealed a reasonably homogeneous distribution of reinforced particles in the matrix.
- Sintering temperature and holding time are the most significant parameters over sintered density. However, the effect of sintering pressure over density is insignificant. The maximum density is achieved at 550 °C with a holding time of 15 min.
- The main effect plot of the Taguchi model suggested that the maximum hardness of composites is achieved at 600 °C and 10 min of holding time.
- The main effect plot of the Taguchi model suggested that the minimum wear loss of composites is achieved at 600 °C, 10 min holding time, and 7 MPa sintering pressure.
- SEM of worn surfaces exhibits that micro-cutting, crates, grooves, and smaller pits are the dominant reason for the wear loss of the composite under a dry sliding environment.

Author Contributions: Conceptualization, A.H.A.; Data curation, A.S.; Formal analysis, M.M.; Investigation, S.A. (Salman Ansari), S.A. (Sajjad Arif) and A.S.; Supervision, S.A. (Sajjad Arif) and A.H.A.; Validation, A.H.A.; Writing—original draft, S.A. (Salman Ansari); Writing—review & editing, S.A. (Sajjad Arif), H.H. and M.M. All authors have read and agreed to the published version of the manuscript.

Funding: This research received no external funding.

Institutional Review Board Statement: Not applicable.

Informed Consent Statement: Not applicable.

Data Availability Statement: Not applicable.

Conflicts of Interest: The authors declare no conflict of interest.

References

1. Mavhungu, S.T.; Akinlabi, E.T.; Onitiri, M.A.; Varachia, F.M. Aluminum Matrix Composites for Industrial Use: Advances and Trends. *Procedia Manuf.* **2017**, *7*, 178–182. [CrossRef]
2. Alam, M.T.; Ansari, A.H.; Arif, S.; Alam, M.N. Mechanical properties and morphology of aluminium metal matrix nanocomposites-stir cast products. *Adv. Mater. Process. Technol.* **2017**, *3*, 600–615. [CrossRef]
3. Alam, M.A.; Ya, H.H.; Azeem, M.; Hussain, P.B.; Salit, M.S.B.; Khan, R.; Arif, S.; Ansari, A.H. Modelling and optimisation of hardness behaviour of sintered Al/SiC composites using RSM and ANN: A comparative study. *J. Mater. Res. Technol.* **2020**, *9*, 14036–14050. [CrossRef]
4. Bodunrin, M.O.; Alaneme, K.K.; Chown, L.H. Aluminium matrix hybrid composites: A review of reinforcement philosophies; Mechanical, corrosion and tribological characteristics. *J. Mater. Res. Technol.* **2015**, *4*, 434–445. [CrossRef]
5. Bhoi, N.K.; Singh, H.; Pratap, S. Developments in the aluminum metal matrix composites reinforced by micro/nano particles—A review. *J. Compos. Mater.* **2020**, *54*, 813–833. [CrossRef]
6. Arif, S.; Jamil, B.; Bilal, M.; Shaikh, N.; Aziz, T.; Ansari, A.H. Characterization of surface morphology, wear performance and modelling of graphite reinforced aluminium hybrid composites. *Eng. Sci. Technol. Int. J.* **2020**, *23*, 674–690. [CrossRef]
7. Reddy, M.P.; Himyan, M.A.; Ubaid, F.; Shakoor, R.A.; Vyasaraj, M.; Gururaj, P.; Yusuf, M.; Mohamed, A.M.A.; Gupta, M. Enhancing thermal and mechanical response of aluminum using nanolength scale TiC ceramic reinforcement. *Ceram. Int.* **2018**, *44*, 9247–9254. [CrossRef]
8. Chaira, D. *Powder Metallurgy Routes for Composite Materials Production*; Elsevier Ltd.: Amsterdam, The Netherlands, 2021; ISBN 9780128035818.
9. Shaikh, M.B.N.; Aziz, T.; Arif, S.; Ansari, A.H.; Karagiannidis, P.G.; Uddin, M. Effect of sintering techniques on microstructural, mechanical and tribological properties of Al-SiC composites. *Surf. Interfaces* **2020**, *20*, 100598. [CrossRef]
10. Mohd Bilal Naim Shaikh, S.A.; Acce, M.A.S. Aluminium and its alloy based composites are widely used in aerospace and automobile d M us pt. *Mater. Res. Express* **2018**, *5*, 829.
11. Awotunde, M.A.; Adegbenjo, A.O.; Obadele, B.A.; Okoro, M.; Shongwe, B.M.; Olubambi, P.A. Influence of sintering methods on the mechanical properties of aluminium nanocomposites reinforced with carbonaceous compounds: A review. *J. Mater. Res. Technol.* **2019**, *8*, 2432–2449. [CrossRef]
12. Ghasali, E.; Pakseresht, A.; Safari-kooshali, F.; Agheli, M.; Ebadzadeh, T. Investigation on microstructure and mechanical behavior of Al-ZrB_2 composite prepared by microwave and spark plasma sintering. *Mater. Sci. Eng. A* **2015**, *627*, 27–30. [CrossRef]
13. Fan, X.; Cai, X.; Rong, Z.; Yang, F.; Li, G.; Gan, Z. Resistance pressing sintering: A simple, economical and practical technique and its application to p-type $(Bi,Sb)_2Te_3$ thermoelectric materials. *J. Alloy. Compd.* **2014**, *607*, 91–98. [CrossRef]
14. Ghasali, E.; Alizadeh, M.; Niazmand, M.; Ebadzadeh, T. Fabrication of magnesium-boron carbide metal matrix composite by powder metallurgy route: Comparison between microwave and spark plasma sintering. *J. Alloy. Compd.* **2017**, *697*, 200–207. [CrossRef]
15. Lagos, M.A.; Agote, I.; Schubert, T.; Weissgaerber, T.; Gallardo, J.M.; Montes, J.M.; Prakash, L.; Andreouli, C.; Oikonomou, V.; Lopez, D.; et al. Development of electric resistance sintering process for the fabrication of hard metals: Processing, microstructure and mechanical properties. *Int. J. Refract. Met. Hard Mater.* **2017**, *66*, 88–94. [CrossRef]
16. Maki, S.; Harada, Y.; Mori, K. Application of resistance sintering technique to fabrication of metal matrix composite. *J. Mater. Process. Technol.* **2001**, *119*, 210–215. [CrossRef]
17. Akhter, H.; Ansari, M.S.J.A. High Current Resistance Sintering For Producing Brass Powder Components. In Proceedings of the 2005 International Conference on Power Electronics and Drives Systems, Kuala Lumpur, Malaysia, 28 November–1 December 2005; pp. 915–919.
18. Cuevas, F.G.; Andreouli, D.; Gallardo, J.M.; Oikonomou, V.; Cintas, J.; Torres, Y.; Montes, J.M. Ceramic dies selection for electrical resistance sintering of metallic materials. *Ceram. Int.* **2019**, *45*, 14555–14561. [CrossRef]
19. Ramakrishnan, D. *Automotive Applications of Powder Metallurgy*; Woodhead Publishing Limited: Sawston, UK, 2013. [CrossRef]

20. Ramesh, C.S.; Khan, A.R.A.; Ravikumar, N.; Savanprabhu, P. Prediction of wear coefficient of Al6061—TiO_2 composites. *Wear* **2005**, *259*, 602–608. [CrossRef]
21. Ravichandran, M.; Naveen Sait, A.; Anandakrishnan, V. Synthesis and forming characteristics of Al–TiO_2 powder metallurgy composites during cold upsetting under plane stress state conditions. *J. Sandw. Struct. Mater.* **2015**, *17*, 278–294. [CrossRef]
22. Kumar, C.A.V.; Rajadurai, J.S. Influence of rutile (TiO_2) content on wear and microhardness characteristics of aluminium-based hybrid composites synthesized by powder metallurgy. *Trans. Nonferrous Met. Soc. China* **2016**, *26*, 63–73. [CrossRef]
23. Guo, M.L.T.; Tsao, C.Y.A. Tribological behavior of self-lubricating aluminium/SiC/graphite hybrid composites synthesized by the semi-solid powder-densification method. *Compos. Sci. Technol.* **2000**, *60*, 65–74. [CrossRef]
24. Salman, S.D.; Leman, Z.B. Physical, mechanical and ballistic properties of kenaf fiber reinforced poly vinyl butyral and its hybrid composites. In *Natural Fibre Reinforced Vinyl Ester and Vinyl Polymer Composites*; Woodhead Publishing: Sawston, UK, 2018; pp. 249–263. [CrossRef]
25. Choudhury, A.; Nanda, J.; Das, S.N. Sintering sensitivity of aluminium metal matrix composites developed through powder metallurgy proposed technique—A review. *J. Phys. Conf. Ser.* **2021**, *2070*, 12193. [CrossRef]
26. Islak, S.; Kir, D.; Buytoz, S. Effect of sintering temperature on electrical and microstructure properties of hot pressed Cu-TiC composites. *Sci. Sinter.* **2014**, *46*, 15–21. [CrossRef]
27. Rahimian, M.; Ehsani, N.; Parvin, N.; reza Baharvandi, H. The effect of particle size, sintering temperature and sintering time on the properties of Al-Al_2O_3 composites, made by powder metallurgy. *J. Mater. Process. Technol.* **2009**, *209*, 5387–5393. [CrossRef]
28. Du, X.; Liu, R.; Xiong, X.; Liu, H. Effects of sintering time on the microstructure and properties of an Al-Cu-Mg alloy. *J. Mater. Res. Technol.* **2020**, *9*, 9657–9666. [CrossRef]
29. Maclin John Vasanth, K.; Lokendar Ram, P.S.; Pon Anand, V.; Prabu, M.; Rahul, S. Experimental investigation of mechanical and tribological properties of Aluminium metal matrix composites fabricated by powder metallurgy route—A review. *Mater. Today Proc.* **2020**, *33*, 1058–1072. [CrossRef]
30. Dixit, M.; Srivastava, R.K. Effect of compaction pressure on microstructure, density and hardness of Copper prepared by Powder Metallurgy route. *IOP Conf. Ser. Mater. Sci. Eng.* **2018**, *377*, 12209. [CrossRef]
31. Garbiec, D.; Siwak, P.; Mróz, A. Effect of compaction pressure and heating rate on microstructure and mechanical properties of spark plasma sintered Ti6Al_4V alloy. *Arch. Civ. Mech. Eng.* **2016**, *16*, 702–707. [CrossRef]
32. Ravi Kumar, K.; Kiran, K.; Sreebalaji, V.S. Micro structural characteristics and mechanical behaviour of aluminium matrix composites reinforced with titanium carbide. *J. Alloy. Compd.* **2017**, *723*, 795–801. [CrossRef]
33. Rahimian, M.; Ehsani, N.; Parvin, N.; Baharvandi, H.R. The effect of sintering temperature and the amount of reinforcement on the properties of Al-Al_2O_3 composite. *Mater. Des.* **2009**, *30*, 3333–3337. [CrossRef]
34. Gürbüz, M.; Can Şenel, M.; Koç, E. The effect of sintering time, temperature, and graphene addition on the hardness and microstructure of aluminum composites. *J. Compos. Mater.* **2018**, *52*, 553–563. [CrossRef]
35. Da Aragão, V.T.S.; Silva, V.S.; de Carvalho, R.R.; Matos, R.S.; Ferreira, N.S.; de Melo, D.M.A.; Oliveira, R.M.P.B. Analyzing coarsening versus densification phenomenon present in partial sintering of Al_2O_3/TiO_2 composites. *J. Mater. Res. Technol.* **2021**, *15*, 2711–2724. [CrossRef]
36. Ghosh, S.K.; Saha, P. Crack and wear behavior of SiC particulate reinforced aluminium based metal matrix composite fabricated by direct metal laser sintering process. *Mater. Des.* **2011**, *32*, 139–145. [CrossRef]
37. Sousa, V.F.C.; Silva, F.J.G.; Alexandre, R.; Fecheira, J.S.; Silva, F.P.N. Study of the wear behaviour of TiAlSiN and TiAlN PVD coated tools on milling operations of pre-hardened tool steel. *Wear* **2021**, *476*, 203695. [CrossRef]
38. Idusuyi, N.; Olayinka, J.I. Dry sliding wear characteristics of aluminium metal matrix composites: A brief overview. *J. Mater. Res. Technol.* **2019**, *8*, 3338–3346. [CrossRef]
39. Gladston, J.A.K.; Dinaharan, I.; Sheriff, N.M.; Selvam, J.D.R. Dry sliding wear behavior of AA6061 aluminum alloy composites reinforced rice husk ash particulates produced using compocasting. *J. Asian Ceram. Soc.* **2017**, *5*, 127–135. [CrossRef]
40. Arif, S.; Alam, M.T.; Ansari, A.H.; Siddiqui, M.A.; Mohsin, M. Study of mechanical and tribological behaviour of Al/SiC/ZrO2 hybrid composites fabricated through powder metallurgy technique. *Mater. Res. Express* **2017**, *4*, 76511. [CrossRef]
41. Arif, S.; Alam, T.; Ansari, A.H.; Shaikh, M.B.N. Morphological characterization, statistical modelling and tribological behaviour of aluminum hybrid nanocomposites reinforced with micro-nano-silicon carbide. *J. Asian Ceram. Soc.* **2019**, *7*, 434–448. [CrossRef]
42. Ravindran, P.; Manisekar, K.; Narayanasamy, P.; Selvakumar, N.; Narayanasamy, R. Application of factorial techniques to study the wear of Al hybrid composites with graphite addition. *Mater. Des.* **2012**, *39*, 42–54. [CrossRef]